Geophysical Research Letters

Supporting information for

On the links between ice nucleation, cloud phase, and climate sensitivity in CESM2

Zachary McGraw[1,2*], Trude Storelvmo[3], Lorenzo Polvani[1,4,5], Stefan Hofer[3], Jonah Shaw[6,7], Andrew Gettelman[8,‡]

1 Department of Applied Physics and Applied Mathematics, Columbia University, New York, NY, USA
2 NASA Goddard Institute for Space Studies, New York, NY, USA
3 Department of Geosciences, University of Oslo, Oslo, Norway
4 Department of Earth and Environmental Sciences, Columbia University, New York, NY, USA
5 Lamont-Doherty Earth Observatory, Columbia University, Palisades, NY, USA
6 Department of Atmospheric and Oceanic Sciences, University of Colorado Boulder, Boulder, CO, USA
7 Cooperative Institute for Research in Environmental Sciences, University of Colorado Boulder, Boulder, CO, USA
8 National Center for Atmospheric Research, Boulder, Colorado
‡ Now at Pacific Northwest National Laboratory, Richland, WA, USA

* corresponding author: zachary.mcgraw@columbia.edu

Contents of this file:

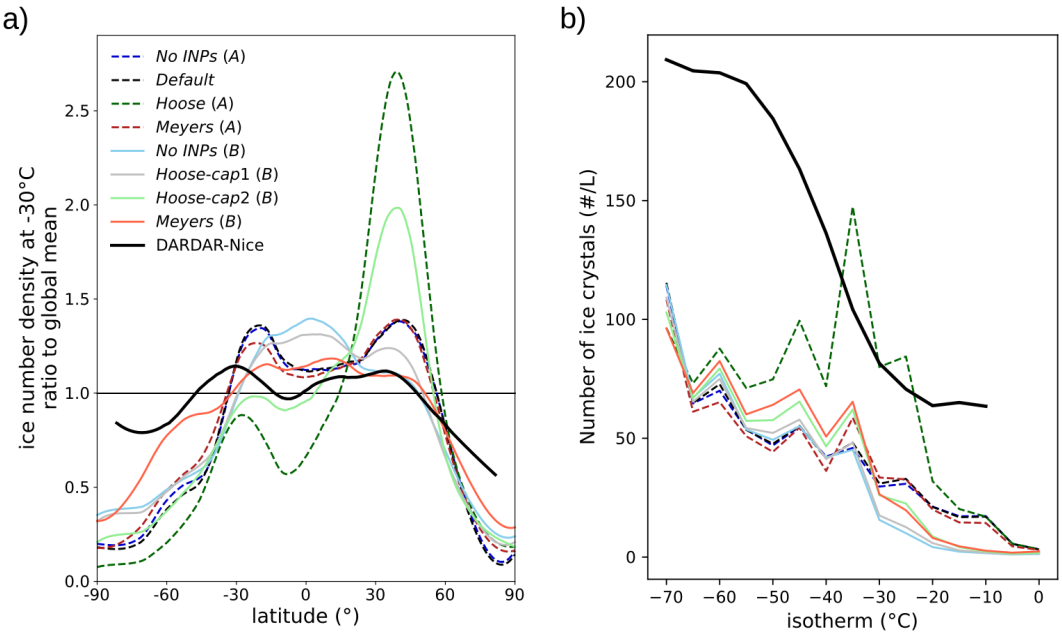

Figure S1 | Ice number density in present-day simulations and DARDAR-Nice satellite retrievals, showing spatial variability of in-cloud ice crystal number near -30°C **(a)** and global mean values across isotherms **(b)**. Data in (a) is normalized by each simulation's global mean value to emphasize differences in spatial structure. This data includes only ice crystals >5μm diameter within ±1°C of each isotherm with gaps of 5°C. To reduce noise in (a), polynomial smoothing was applied using a window of 20° latitude.

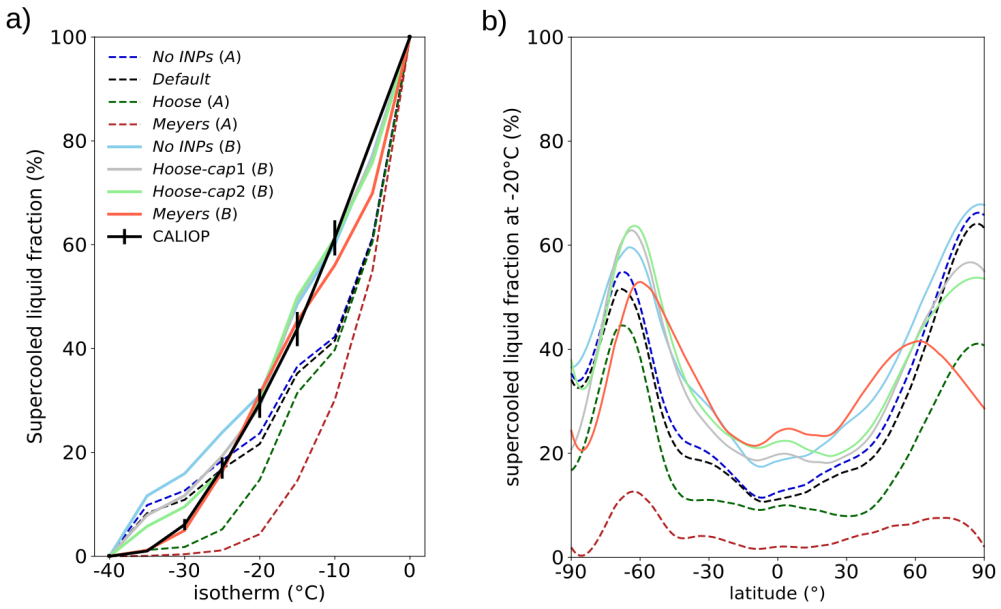

Figure S2 | Supercooled liquid fraction in present-day simulations and CALIOP retrievals, shown by isotherm **(a)** and also by latitude for the -20°C isotherm **(b)**. Only clouds visible to CALIOP are shown, such that clouds under optically thick cloud layers (optical depth τ>3) are ignored. Global mean values are in Table 1. As in Fig. S1a, polynomial smoothing was applied to (b) using a window of 20° latitude.

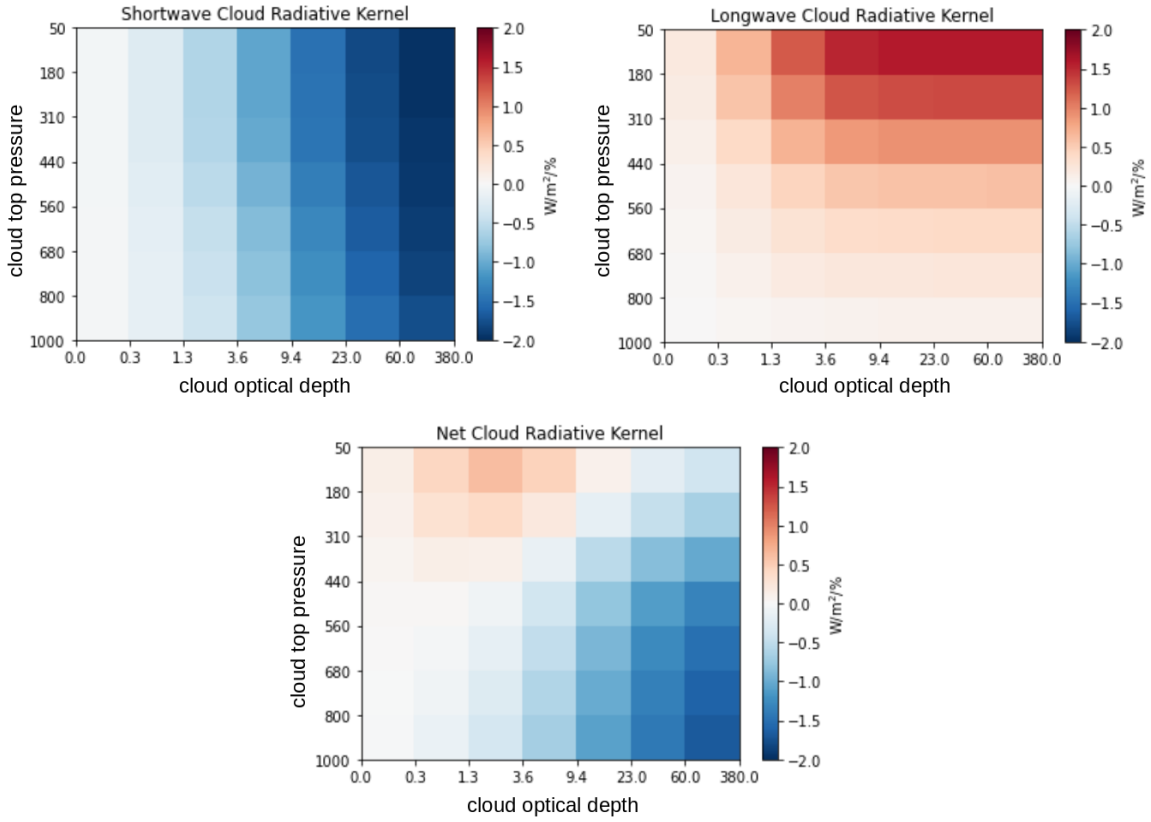

Figure S3 | Radiative kernels used in this study, showing impacts of % changes of each cloud type on shortwave (SW), longwave (LW), and net (SW+LW) radiation. This is as in Fig. 1 of Zelinka et al. (2012a), but here SW influence is averaged over surface albedo data from default CESM2.

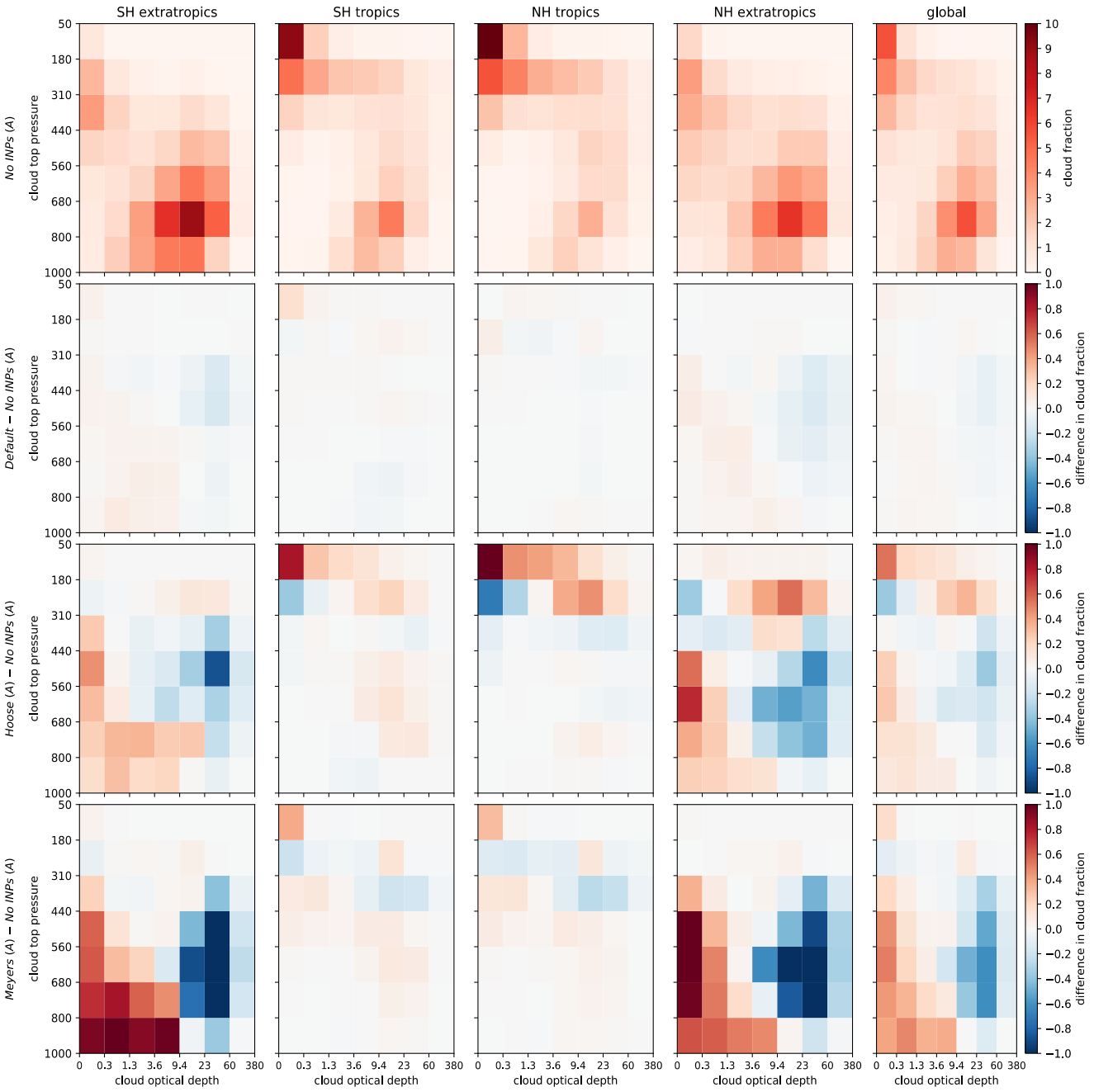

Figure S4 | Cloud types identified in ISCCP cloud histograms, showing changes to prevalence of 49 cloud types. Cloud types are separated by cloud top pressure and optical depth and are shown as standard output for comparison with ISCCP. Output from *No INPs (A)* is shown directly, while the other unadjusted experiments are shown as difference from these cases for clarity. Note that the difference plots have a color bar ten times stronger than those for *No INPs (A)*. Group B experiments are shown separately in Fig. S5.

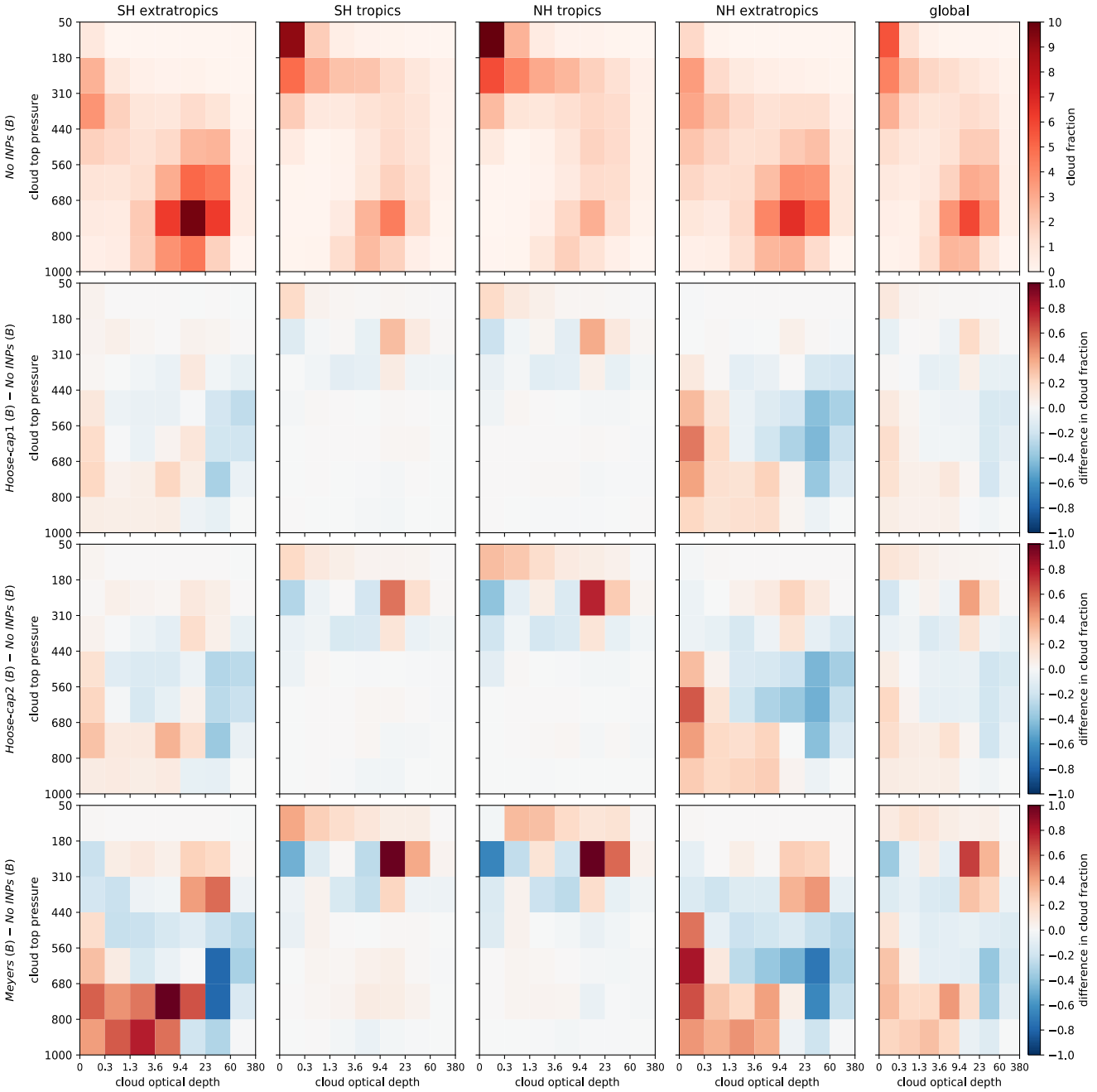

Figure S5 | as in Figure S4 but among the Group B simulations, with experiments here compared to *No INPs (B)*.

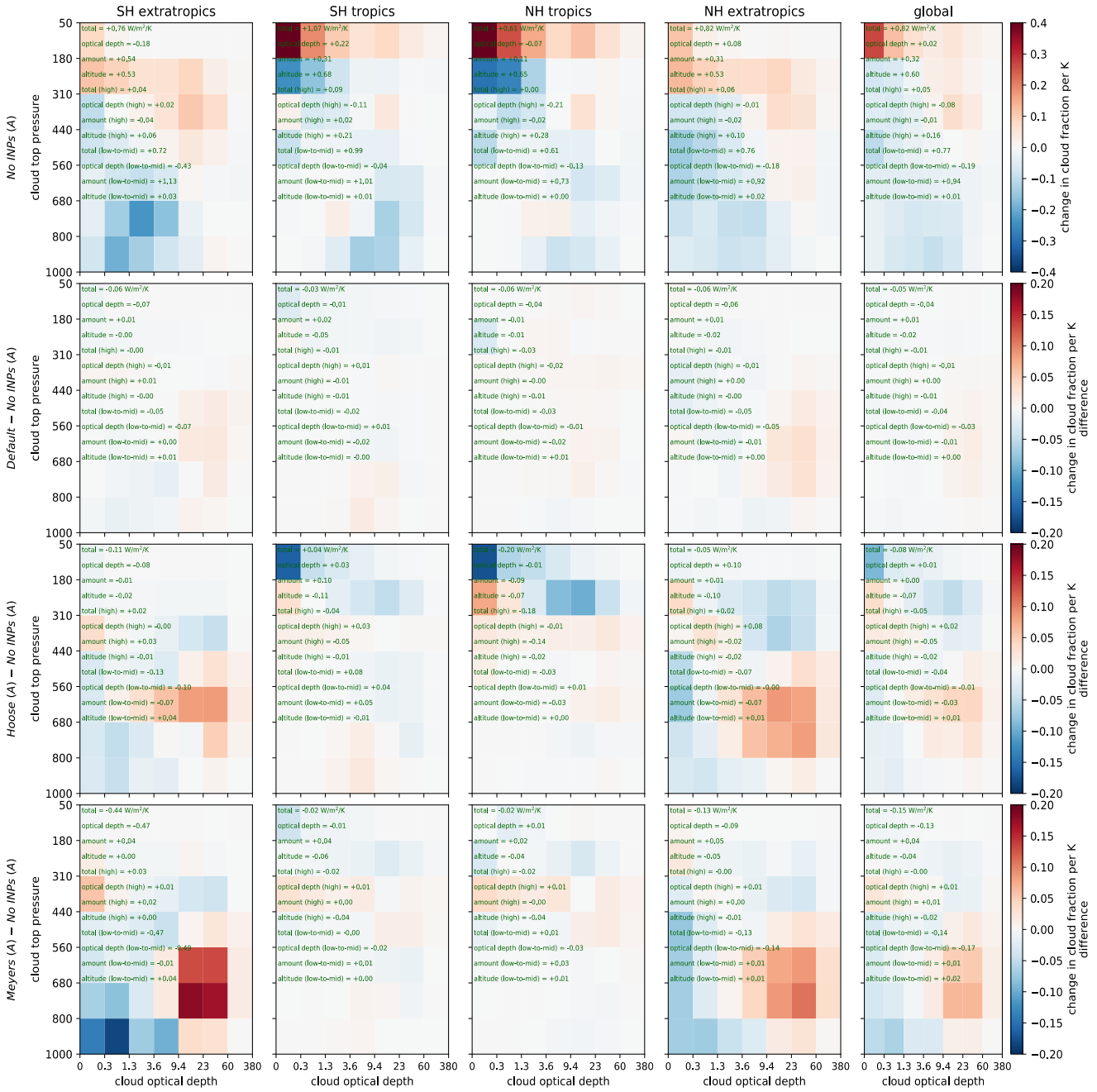

Figure S6 | Cloud changes as warming occurs as identified in ISCCP cloud histograms. Aside for the top row (*No INPs (A, SST+4K) – No INPs (B, present-day)*), the data is shown as four-way differences, i.e. (*experiment*(A, SST+4K) – *experiment(A, present-day)*) – (*No INPs (B, SST+4K) – No INPs (B, present-day)*). Also included on the plots in green text are cloud feedbacks calculated by the kernel method (showing feedback differences compared to *No INPs (A)* below the first row), with low and mid-level clouds grouped together to conserve space. Note that the four-way difference plots have a colorbar twice as strong as the top row. For differences in present-day clouds among the same simulations, see Fig. S4.

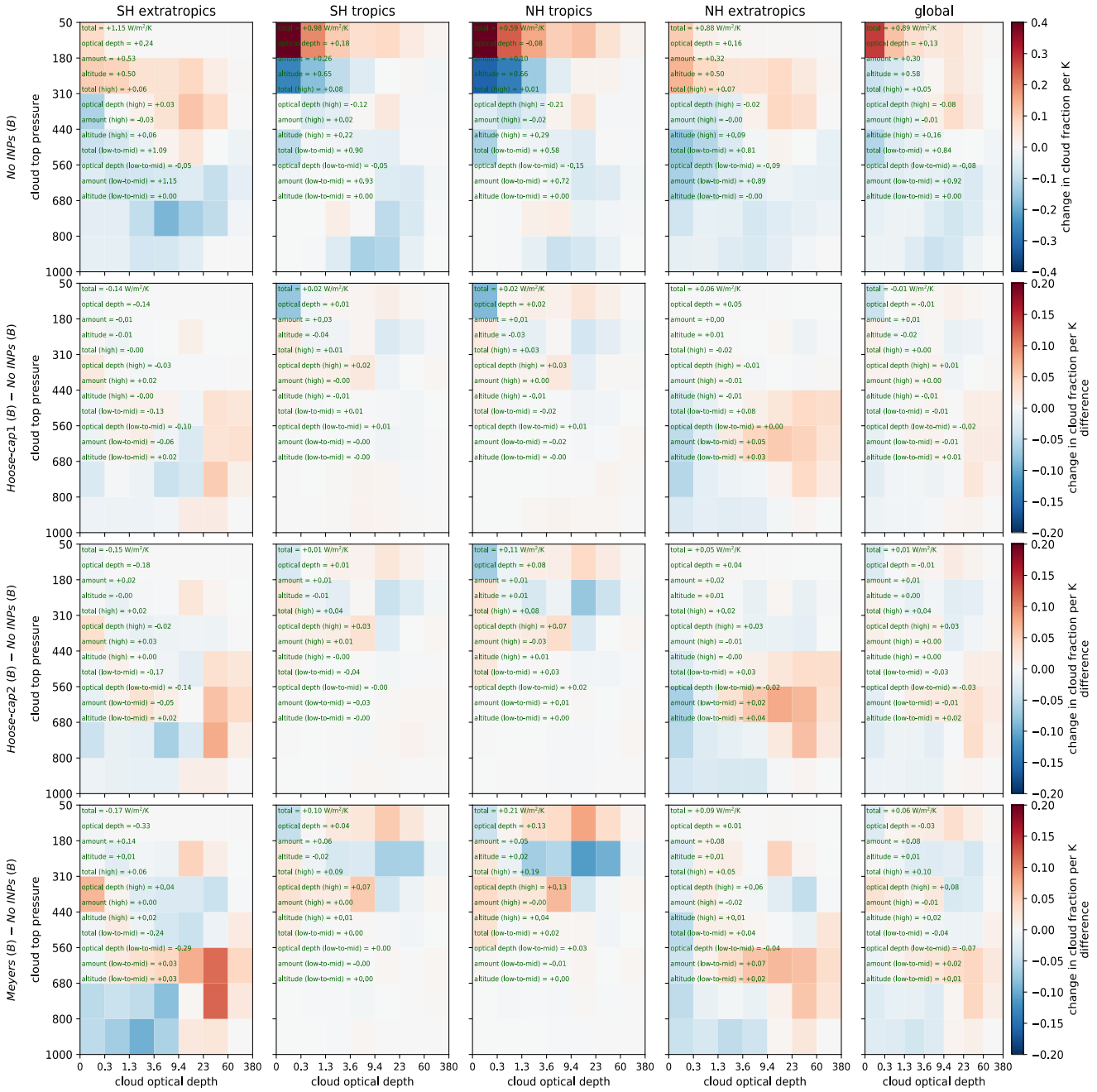

Figure S7 | as in Figure S6 but among the Group B simulations, with experiments being compared to *No INPs (B)*. For differences in present-day clouds among the same experiments, see Fig. S5.

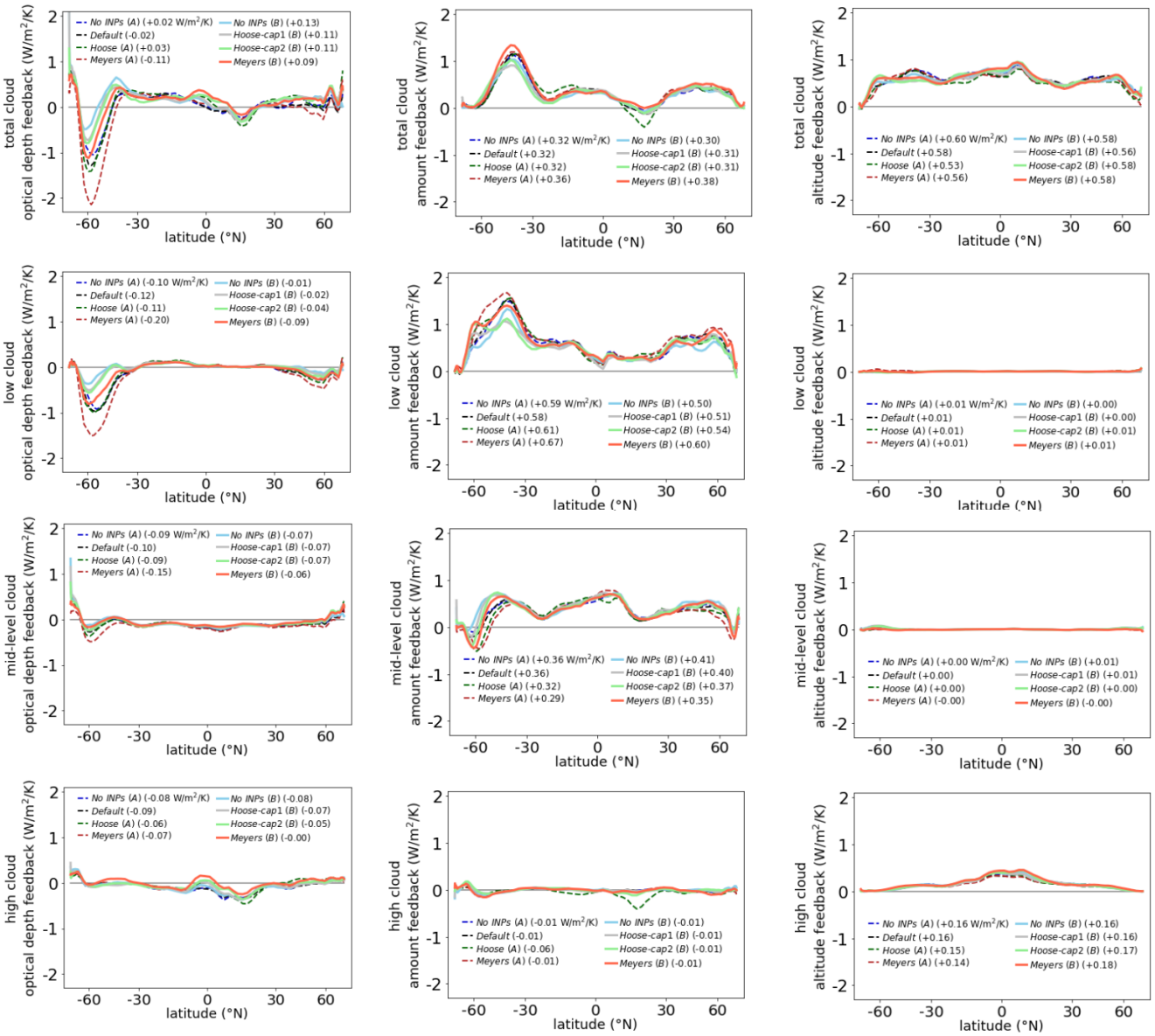

Figure S8 | Cloud feedbacks separated by mechanism in all CESM2 simulations, as in Fig. 3b but further partitioned by mechanism. Global mean feedback values are included in each legend. Note that some mismatch exists between the sum of feedbacks between levels and each unseparated feedback (Zelinka et al., 2016), shown here in the top row.

Supplementary References

Zelinka, M. D., Klein, S. A., & Hartmann, D. L. (2012). Computing and Partitioning Cloud Feedbacks Using Cloud Property Histograms. Part II: Attribution to Changes in Cloud Amount, Altitude, and Optical Depth. *Journal of Climate*, *25*(11), 3736–3754. https://doi.org/10.1175/JCLI-D-11-00249.1

Zelinka, M. D., Zhou, C., & Klein, S. A. (2016). Insights from a refined decomposition of cloud feedbacks. *Geophysical Research Letters*, *43*(17), 9259–9269. https://doi.org/10.1002/2016GL069917